Periodic Attitude Control of a Slowly Spinning Spacecraft

ERNEST P. TODOSIEV*
TRW Systems, Redondo Beach, Calif.

A periodic attitude control system is presented which permits control of secular errors of a slowly spinning spacecraft operating in a high disturbance environment. Attitude errors of the spin-axis are detected by sun sensors (or rate gyros) and are controlled by a periodic control law which modulates external control torques generated by mass expulsion torquers. Attitude stability during the uncontrolled periods is obtained passively via the vehicle spin momentum. Equations of motion, a system block diagram, and design parameters are presented for a typical spacecraft application. Simulation results are included which demonstrate the feasibility of the novel control concept. Salient features of the periodic control approach are implementation simplicity, excellent response, and a propellant utilization efficiency greater than 75%.

Introduction

THE spin-axis error of a spinning vehicle is conventionally controlled by applying a known increment of angular momentum to the vehicle which causes the spacecraft to nutate about a new axis in inertial space.[1,2] A nutation damper (usually of the viscous ring type) is then employed to remove the nutational energy imparted by the precessional maneuver and upon convergence, the vehicle motion is one of pure spin about the new inertial axis.[3,4] As the energy removal capability of the damper is limited, a large number of spacecraft spin revolutions must occur (e.g., a few hundred) before all the nutational energy is removed. The conventional technique is commonly employed on rapidly spinning spacecraft operating in low disturbance environments. As the external disturbances are small, infrequent secular error corrections are required and thus there are no severe constraints on the convergence period of the control interval.

For a spacecraft operating in a high disturbance environment, frequent corrections of the secular error are required. The control problem is further complicated if the vehicle spin rate is low compared to the required control frequency. Conventional control of the spin-axis attitude via vehicle precession and subsequent removal of the nutational energy with a wobble damper is not applicable as the damping interval is unacceptably long. The periodic control concept provides active control for short intervals during which the secular momentum is removed and the spin-axis is realigned with its nominal position.†

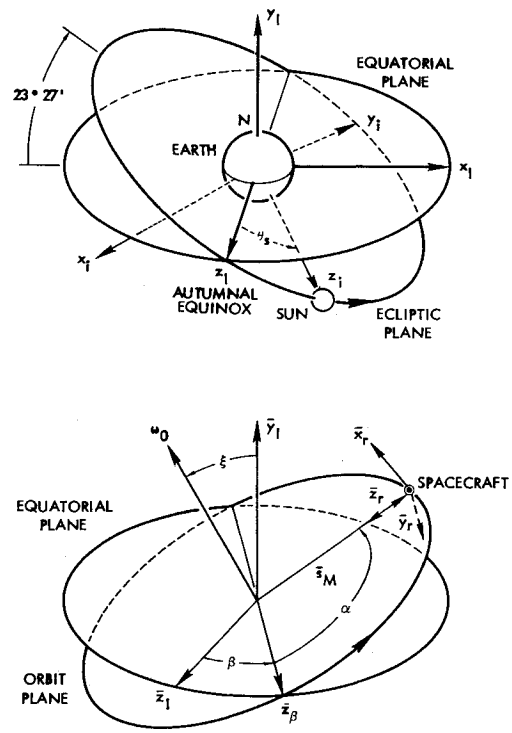

Fig. 1 Definition of coordinate frames and orbital parameters.

Equations of Motion

The vehicle rotational motion is referenced to a quasi-inertial right-handed orthogonal frame (x_i, y_i, z_i) as shown in Fig. 1 where the x_i axis is normal to the ecliptic plane, y_i is within the ecliptic plane, z_i points toward the sun, and the origin is at the Earth's center of mass. Define a body-fixed orthogonal frame (x_b, y_b, z_b) with origin at the spacecraft center of mass and the axes coincident with the principal axes of inertia (Fig. 2). For ideal control (solar array normal to the sun) and the spin angle (ψ) equal to zero, the x_b axis is normal to the ecliptic plane, y_b is parallel to the ecliptic plane, and z_b points towards the sun.

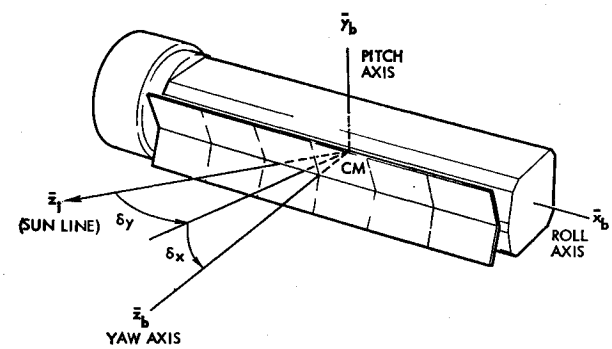

Fig. 2 Definition of control axes and sun pointing errors (δ_x and δ_y).

Presented as Paper 73-246 at the AIAA 11th Aerospace Sciences Meeting, Washington, D.C., January 10–12, 1973; submitted February 8, 1973, revision received July 23, 1973. This work was performed in part during the initial studies of the High Energy Astronomy Observatory under Contract NAS 8-26273 with the NASA Marshall Space Flight Center.

Index category: Spacecraft Attitude Dynamics and Control.

* Project Engineer, HEAO Program Office, Space Vehicles Division. Associate Fellow AIAA.

† Use of periodic control for secular error management was first suggested by H. A. Lassen of the Science and Application Satellite Operations at TRW Systems during preliminary studies on the HEAO program.

Define the spacecraft attitude relative to the quasi-inertial frame (x_i, y_i, z_i) by three ordered rotations; a pitch rotation (θ) about y_i, a roll rotation (ϕ) about the intermediate axis x_i', and a yaw rotation (ψ) about z_b. The spacecraft attitude is then specified by

$$\begin{Bmatrix}\bar{x}_b\\ \bar{y}_b\\ \bar{z}_b\end{Bmatrix} = \begin{bmatrix}b_{11} & b_{12} & b_{13}\\ b_{21} & b_{22} & b_{23}\\ b_{31} & b_{32} & b_{33}\end{bmatrix}\begin{Bmatrix}\bar{x}_i\\ \bar{y}_i\\ \bar{z}_i\end{Bmatrix} \tag{1}$$

where

$$\begin{aligned}
b_{11} &= \cos\psi\cos\theta + \sin\psi\sin\theta\sin\phi\\
b_{12} &= \sin\psi\cos\phi\\
b_{13} &= -\cos\psi\sin\theta + \sin\psi\sin\phi\cos\theta\\
b_{21} &= -\sin\psi\cos\theta + \cos\psi\sin\theta\sin\phi\\
b_{22} &= \cos\phi\cos\psi\\
b_{23} &= \sin\theta\sin\psi + \cos\psi\sin\phi\cos\theta\\
b_{31} &= \sin\theta\cos\phi\\
b_{32} &= -\sin\phi\\
b_{33} &= \cos\phi\cos\theta
\end{aligned} \tag{2}$$

During the celestial scan mode, the attitude errors θ and ϕ are small and consequently the spacecraft attitude can be specified as

$$\begin{Bmatrix}\bar{x}_b\\ \bar{y}_b\\ \bar{z}_b\end{Bmatrix} = \begin{bmatrix}\cos\psi & \sin\psi & -\theta\cos\psi + \phi\sin\psi\\ -\sin\psi & \cos\psi & \theta\sin\psi + \phi\cos\psi\\ \theta & -\phi & 1\end{bmatrix}\begin{Bmatrix}\bar{x}_i\\ \bar{y}_i\\ \bar{z}_i\end{Bmatrix} \tag{3}$$

Define the spacecraft momentum ($\bar{H}_b$), angular velocity ($\bar{\omega}_b$), and external torque ($\bar{T}$) as

$$\begin{aligned}
\bar{H}_b &= H_x\bar{x}_b + H_y\bar{y}_b + H_z\bar{z}_b\\
\bar{\omega}_b &= \omega_x\bar{x}_b + \omega_y\bar{y}_b + \omega_z\bar{z}_b\\
\bar{T} &= T_x\bar{x}_b + T_y\bar{y}_b + T_z\bar{z}_b
\end{aligned} \tag{4}$$

By Newton's law, the spacecraft equation of motion is

$$d/dt(\bar{H}_b) = \bar{T} \tag{5}$$

Assuming negligible inertia cross-products yields the following scalar equations of motion:

$$\begin{aligned}
I_{xx}\dot{\omega}_x - (I_{yy} - I_{zz})\omega_y\omega_z &= T_x\\
I_{yy}\dot{\omega}_y - (I_{zz} - I_{xx})\omega_z\omega_x &= T_y\\
I_{zz}\dot{\omega}_z - (I_{xx} - I_{yy})\omega_x\omega_y &= T_z
\end{aligned} \tag{6}$$

Ignoring the Earth's orbit rate about the sun (1°/day), the spacecraft angular velocity can also be defined as

$$\bar{\omega}_b = \dot{\theta}\bar{y}_i + \dot{\phi}\bar{x}_i' + \dot{\psi}\bar{z}_b \tag{7}$$

where x_i' is a unit vector defining the location of $\bar{x}_i$ if (x_i, y_i, z_i) were to undergo a pitch rotation (θ). It can be shown that

$$\begin{aligned}
\dot{\phi} &= \omega_x\cos\psi - \omega_y\sin\psi\\
\dot{\theta} &= (1/\cos\phi)[\omega_x\sin\psi + \omega_y\cos\psi]\\
\dot{\psi} &= \omega_z + \dot{\theta}\sin\phi
\end{aligned} \tag{8}$$

For small pitch and roll angles, the body velocity components can be expressed as

$$\begin{aligned}
\omega_x &= \dot{\phi}\cos\psi + \dot{\theta}\sin\psi\\
\omega_y &= \dot{\theta}\cos\psi - \dot{\phi}\sin\psi\\
\omega_z &= \dot{\psi}
\end{aligned} \tag{9}$$

To facilitate development of the small-angle equations of motion, define a "despun" coordinate frame (x_d, y_d, z_d) by the matrix equation

$$\begin{Bmatrix}\bar{x}_d\\ \bar{y}_d\\ \bar{z}_d\end{Bmatrix} = \begin{bmatrix}\cos\psi & -\sin\psi & 0\\ \sin\psi & \cos\psi & 0\\ 0 & 0 & 1\end{bmatrix}\begin{Bmatrix}\bar{x}_b\\ \bar{y}_b\\ \bar{z}_b\end{Bmatrix} \tag{10}$$

Transforming Eq. (6) to the despun frame, yields the following small-angle equations of motion:

$$\begin{aligned}
&I_{xx}\{\ddot{\phi}\cos^2\psi + (\ddot{\theta}/2)\sin2\psi + \dot{\psi}(\dot{\theta}\cos2\psi - \dot{\phi}\sin2\psi)\}\\
&\quad - I_{yy}\{(\ddot{\theta}/2)\sin2\psi - \ddot{\phi}\sin^2\psi + \dot{\psi}(\dot{\theta}\cos2\psi - \dot{\phi}\sin2\psi)\}\\
&\quad + I_{zz}\dot{\theta}\dot{\psi} = T_x\cos\psi - T_y\sin\psi\\
&I_{xx}\{(\ddot{\phi}/2)\sin2\psi + \ddot{\theta}\sin^2\psi + \dot{\psi}(\dot{\phi}\cos2\psi + \dot{\theta}\sin2\psi)\}\\
&\quad + I_{yy}\{\ddot{\theta}\cos^2\psi - (\ddot{\phi}/2)\sin2\psi - \dot{\psi}(\dot{\phi}\cos2\psi + \dot{\theta}\sin2\psi)\}\\
&\quad - I_{zz}\dot{\phi}\dot{\psi} = T_x\sin\psi + T_y\cos\psi\\
&I_{zz}\ddot{\psi} = T_z
\end{aligned} \tag{11}$$

The spacecraft spin rate ($\dot{\psi}$) produces severe coupling between the roll and pitch axes. This coupling together with the transcendental terms produces a complex spacecraft motion which is difficult to analyze. For an asymmetrical spacecraft at an orbital altitude of 200 naut miles, the gravity gradient torque is the major external disturbance torque. Since the yaw component of this torque (T_z) has an average value of zero over any spacecraft spin period (as derived in the Appendix), the spin rate ($\dot{\psi}$) deviation is small. For the candidate spacecraft, the spin rate derivation was less than 1%, and consequently the spin rate was assumed constant at a value of ω_s rad/sec. With this simplification, the roll and pitch equations of motion can be written in the compact matrix form

$$\begin{bmatrix}Dp^2 + Ep & Fp^2 + Gp\\ Fp^2 + Hp & Jp^2 - Ep\end{bmatrix}\begin{Bmatrix}\phi\\ \theta\end{Bmatrix} = \begin{Bmatrix}T_x'\\ T_y'\end{Bmatrix} \tag{12}$$

where

$$\begin{aligned}
D &= I_{xx}\cos^2\psi + I_{yy}\sin^2\psi\\
E &= (I_{yy} - I_{xx})\omega_s\sin2\psi\\
F &= \tfrac{1}{2}(I_{xx} - I_{yy})\sin2\psi\\
G &= (I_{xx}\cos2\psi - I_{yy}\cos2\psi + I_{zz})\omega_s\\
H &= (I_{xx}\cos2\psi - I_{yy}\cos2\psi - I_{zz})\omega_s\\
J &= I_{xx}\sin^2\psi + I_{yy}\cos^2\psi\\
\psi &= \omega_s t\\
T_x' &= T_x\cos\psi - T_y\sin\psi\\
T_y' &= T_x\sin\psi + T_y\cos\psi
\end{aligned} \tag{13}$$

and p is the operator d/dt.

From the Appendix, the roll and pitch gravity gradient torques (i.e., the dominant external torques) are

$$\begin{aligned}
T_x &= K(I_{zz} - I_{yy})y_{33}(y_{32}\cos\psi - y_{31}\sin\psi)\\
T_y &= K(I_{xx} - I_{zz})y_{33}(y_{31}\cos\psi + y_{32}\sin\psi)
\end{aligned} \tag{14}$$

where K, y_{31}, y_{32}, and y_{33} are functions of the orbital parameters. The equations of motion defined by Eqs. (12) and (13) possess time-variable-parameters and can be most expeditiously studied via digital simulation.

Control Concept

The periodic attitude control system provides control of a slowly spinning spacecraft in a low Earth orbit with a control interval which is only a fraction of the spin period. Secular spin-axis errors due to the dominant gravity gradient disturbance torque are periodically detected by sun sensors and removed via modulation of mass expulsion thrusters according to a novel automatic control law which minimizes the interaxis coupling and ensures convergence within half a spin period. Damping is provided by rate gyros. The spacecraft spin speed must be initially adjusted to give an integral number of spacecraft revolutions per orbit. Control action may be taken as often as once per spin period. Attitude errors of the spin-axis attitude at the end of each control interval are primarily determined by the sun sensors and control accuracies of less than 1° are readily achievable. Spin-axis errors during the uncontrolled periods are determined by the vehicle momentum and the magnitude of the external disturbance torques. Attitude stability during this period is obtained passively via the vehicle spin momentum.

Consider a specific application where it is required to orient the spacecraft spin-axis (i.e., the z axis) toward the sun. Two sun sensors are employed to measure the spacecraft attitude error; one measures the sun pointing error in the body $x_b z_b$ plane and the other measures the error in the body $y_b z_b$ plane (Fig. 2). Ideally the sun sensor outputs (μ_x and μ_y) are defined by the vector dot products

$$\begin{aligned} \mu_x &= \bar{y}_b \cdot \bar{z}_i = \sin\delta_x \\ \mu_y &= \bar{x}_b \cdot \bar{z}_i = -\sin\delta_y \end{aligned} \tag{15}$$

and for small pointing errors, the sensor outputs reduce to

$$\begin{aligned} \mu_x &= \delta_x \\ \mu_y &= -\delta_y \end{aligned} \tag{16}$$

The orthogonal components of the sun pointing error in body coordinates (δ_x and δ_y) are related to the inertial attitude errors by the following equations:

$$\begin{aligned} \delta_x &= \phi\cos\psi + \theta\sin\psi \\ \delta_y &= -\phi\sin\psi + \theta\cos\psi \end{aligned} \tag{17}$$

The sun pointing error rate components are also related to the inertial rate components via the following equations:

$$\begin{aligned} \dot{\delta}_x &= \omega_x + \dot{\psi}\delta_y \\ \dot{\delta}_y &= \omega_y - \dot{\psi}\delta_x \end{aligned} \tag{18}$$

Processing of the rate gyro outputs (ideally ω_x, ω_y, ω_z) according to Eq. (18) and integrating yields the sun pointing error components. Therefore equivalent sun sensor outputs can be readily derived from the rate gyros. This fact greatly simplifies the derivation of the attitude errors during eclipse and when it is required to orient the spacecraft spin-axis in a nonsolar direction.

System Design

The control design operates in three basic modes: 1) sun acquisition in which the spacecraft is oriented such that the body-fixed array points at the sun, 2) celestial scan in which the spacecraft slowly rotates at 0.1 rpm about the z axis which is controlled to point at the sun, and 3) offset celestial scan where the scan motion about the z axis is maintained but about a new reference axis offset as much as 30° from the sun.

Sun Acquisition

The sun acquisition mode (Mode 1) is shown functionally in Fig. 3 and is a conventional rate plus position system where position data is derived from sun sensors and rate data from gyros. The position and rate control gains are donoted by K_P and K_R, respectively. Acquisition from any attitude is assured via the coarse sun sensor which has a 4π steradian field of view. Control is automatically transferred to the fine sun sensors for small sun pointing errors. Employment of the rate gyros for damping ensures convergence from arbitrarily high initial tipoff rates. Upon convergence in the sun acquisition mode, the spacecraft xy plane will be normal to the sun line with the rate about the z axis controlled to be less than 6.55×10^{-3} deg/sec.

Roll and pitch convergence from large errors proceeds at a fixed slew rate determined by the rate gain and the saturation level of the sun sensor signal. A saturation level of 20° and a rate gain of 20° per deg/sec yields a design slew rate of 1°/sec. The resultant worst-case single axis acquisition (from an attitude error of 180°) is approximately 3 min, thus permitting the sun acquisition maneuver to be performed when the spacecraft is in sight of a ground station; simulation data indicates a 5 min three-axis acquisition time for this extreme case. Table 1 lists the control parameters for the sun acquisition mode. Control torques for the sun acquisition mode and the scan modes are 7.5, 22.5, and 22.5 ft lb about the vehicle roll, pitch, and yaw axes, respectively.

Periodic Celestial Scan

The periodic celestial scan mode (Mode 2) provides two control intervals per orbit with the spin momentum providing moderate stiffness between resets. In this mode, the nominal

Table 1 Control parameters for sun acquisition

Axis	Control deadzone (deg)	Position gain (deg/deg)	Rate gain (sec)	Modulator hysteresis (percent)
Roll	0.4	1	20	20
Pitch	0.4	1	20	20
Yaw	0.4[a]	0	61[a]	95

[a] Yields a rate deadzone of 0.0011 rpm.

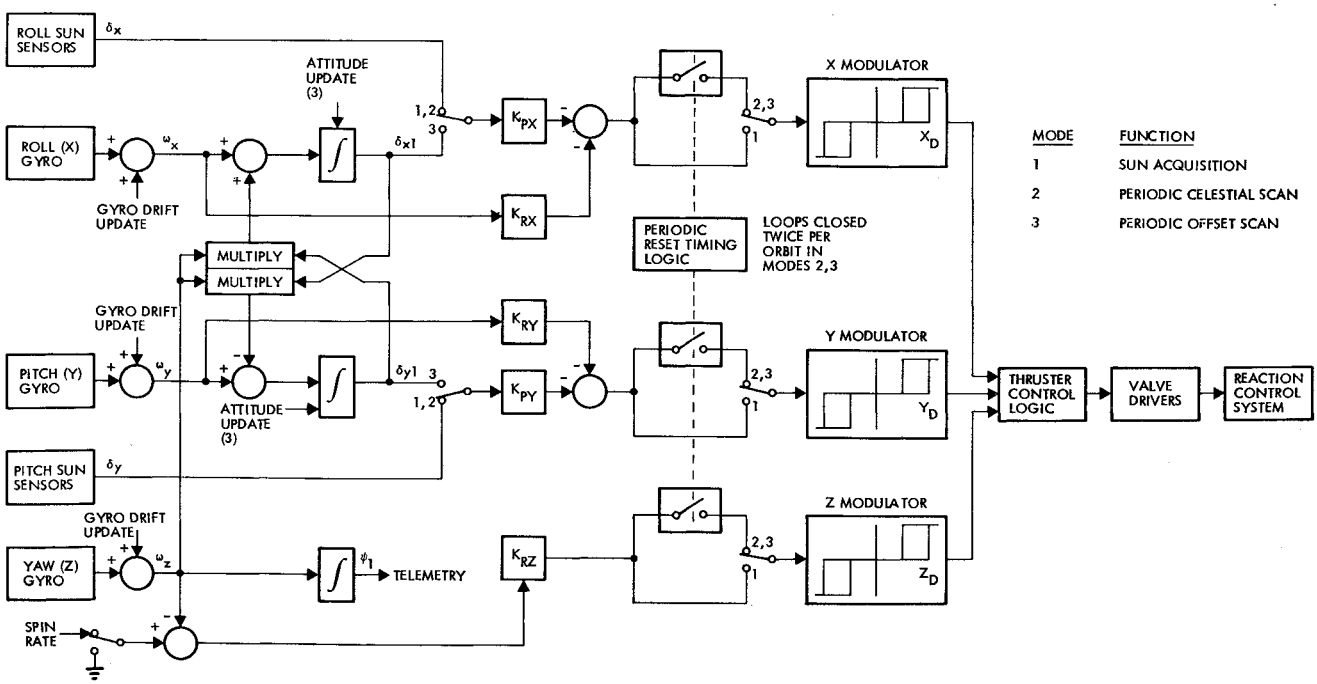

Fig. 3 Block diagram of periodic attitude controlsystem.

spacecraft spin rate is selected to give an integral number of spacecraft revolutions in each orbit. The resultant spacecraft motion, under the influence of gravity gradient torques, repeats approximately every half orbit. Near the end of each half orbit, the control system is activated and employed to reduce the spacecraft sun pointing error to the deadzone values of $\pm 0.4°$ about the spacecraft z and y axes. During the control interval, the spacecraft spin speed is also corrected to within 0.1% of the reference spin rate. A control interval of 200 sec is employed, and upon completion of the control maneuver, the attitude control loops are opened. The spacecraft motion during the subsequent half orbit differs slightly from the motion of the preceding half orbit because of the influence of the spacecraft initial attitude and attitude rates which are a function of the control deadzone and the limit cycle rates.

Major considerations in the periodic celestial scan design are: 1) maximization of control efficiency in terms of propellant usage, 2) minimization of the control period and the number of thruster firings, and 3) minimization of dynamic coupling between the x and y axes. Criteria (1) and (3) are realized by initiating the control maneuver when the spacecraft is at that specific point in its nutational motion where the pitch/roll attitude error exists solely about the roll axis. At that instant the spacecraft x axis is normal to the spacecraft-sun line. This point is readily detectable via the y sun sensor which measures the sun pointing error in the body xz plane, so that at the time attitude control is initiated (i.e., at $\delta_y = 0 \pm 0.5°$), the pitch/roll attitude is primarily in roll. The resultant control efficiency is better than 75% for the peak secular gravity gradient torque.

In this mode, the roll sun sensor output is limited at 1° yielding a modulator switching zone which produces an approximately constant attitude slew rate during the convergence period. This design feature substantially reduces the number of thruster firings and also increases the efficiency of the control maneuver.

The specific control system parameters for periodic control during celestial scan are shown in Table 2. Spin speed is controlled to within 0.1% of the nominal spin rate (0.109 rpm).

The periodic attitude control system is armed at two points 180° apart in the orbit. These arming points are referenced to sunrise in each orbit and are specified by a clock. Each control interval is initiated (after being armed) at the next zero crossing of the pitch sun sensor and is 200 sec long (which is equivalent to 13.1° of orbit angle). The sensor zero crossings occur every half spacecraft spin period or every 18° of orbit angle.

Periodic Offset Scan

During celestial scan, the nominal position of the scan axis is the sun line. Angular errors relative to the sun line are measured with two orthogonal sun sensors. In the offset scan mode (Mode 3), the reference spin axis is offset from the sun line and spacecraft attitude errors relative to the new reference must now be derived. The error-derivation approach selected is based on processing the rate gyro data to yield orthogonal errors about the x and y axes which are referenced to the offset reference spin axis. Error accumulation is corrected when necessary by ground computed attitude (obtained from a star tracker) and drift bias updates. Note that the yaw attitude signal (ψ_1 in Fig. 3) is generated to be telemetered for update computation even though it is not used for control in this mode. The gyro processing scheme is analogous to two orthogonal sun sensors viewing a fictitious sun located on the offset scan axis. Consequently, the control laws derived for periodic control in the scan mode can be employed without change in the offset scan mode.

In the nomenclature of the functional block diagram of the previous section, the simulated sun sensor outputs are generalized from

$$\begin{aligned} \dot{\delta}_{x1} &= \omega_x + \dot{\psi}\delta_{y1} \\ \dot{\delta}_{y1} &= \omega_y - \dot{\psi}\delta_{x1} \end{aligned} \tag{19}$$

These equations can be integrated to yield δ_{x1} and δ_{y1} as shown in Fig. 3.

Table 2 Control parameters for periodic celestial scan

Axis	Control deadzone (deg)	Position gain (deg/deg)	Rate gain (sec)	Modulator hysteresis (percent)
Roll	0.4	1	30	95
Pitch	0.4	1	30	95
Yaw	0.4[a]	0	610[a]	95

[a] Yields a rate deadzone of 0.00011 rpm (0.1 percent of bias).

System Performance

Sun Acquisition

Performance of the sun acquisition system was ascertained via a digital simulation. The initial spacecraft attitude was selected to give a worst case initial error of 180° by orienting the spacecraft z axis to point directly away from the sun. Initial rates of 1°/sec were assumed about each spacecraft axis. The spacecraft moments of inertia were 4824, 77140, and 78214 slug-ft² about the x, y, z spacecraft axes. The spacecraft satisfactorily acquired the sun within 250 sec as shown in Fig. 4, where the sun pointing errors are specified by the vector dot products $\bar{x} \cdot \bar{z}_i$ and $\bar{y} \cdot \bar{z}_i$. Rates about the x, y, and z axes are specified by the variables ω_x, ω_y, and ω_z.

Scan Modes

A digital spacecraft simulation was employed to determine the effect of the periodic attitude control system on the spacecraft motion during the celestial scan modes. Note that performance in offset scan will be the same as in celestial scan. The spacecraft orbit was assumed circular with an altitude of 200 naut miles and an inclination of 28.5°. Nodal regression of the orbit was included in the simulation as well as rotation of the spacecraft in its orbit and the rotation of

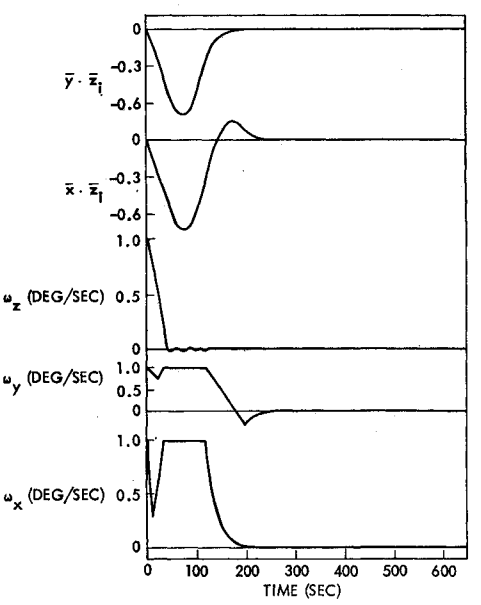

Fig. 4 Sun acquisition performance.

the Earth about the sun. The gravity gradient torque experienced by the spinning spacecraft was also simulated without simplifying approximations. Other disturbances (e.g., magnetic torques, aerodynamic torques, solar pressure torques) have been shown by analysis to be inconsequential compared to gravity gradient torques. Therefore, the simulation included the major disturbance forces which could perturb the spacecraft rotational motion. The spacecraft moments of inertias used in the simulation were 4580, 53700, and 55700 slug-ft^2 about the x, y, and z axes.

The spacecraft orbital parameters were selected to produce a maximum secular gravity gradient torque on the vehicle. A derivation of the secular gravity gradient torque is given in the Appendix. This torque precesses the spacecraft spin axis (z_b) at a rate of about 10°/hr and provides a worst case operational condition for the attitude control system which only corrects the spin-axis attitude every half orbit or 46 min. For other orbital parameters, the secular component of the gravity gradient torque is less severe and when the sunline (i.e., the line between the spacecraft and the sun) lies within the orbit plane, this component is zero. The Appendix contains the explicit functional relationships between the orbital parameters which maximize and minimize the secular component as well as a graph of the normalized secular component (Fig. 9) for orbital parameters between these extremes. The remanent portion of the gravity gradient torque is cyclic in nature with a frequency of twice the spin period. This torque component causes the spacecraft to nutate about the sunline with a small amplitude but with no secular buildup.

During periodic celestial scan, the control system is activated every half orbit for a period of 200 sec to realign the scan-axis to the sunline within the control deadband of ±0.4° about the x_b and y_b spacecraft axes. The performance of the periodic control system is illustrated in Fig. 5, which represents the attitude error time history of the spacecraft z_b axis for 200 min. of simulated operation. During each of the four control periods shown, the attitude control system satisfactorily reduced the scan-axis errors to within the control deadband of ±0.4°. During this period, the spin rate (ω_z) is also controlled as illustrated in Fig. 6 which also shows the transverse body rates ω_x and ω_y. Note that the uncontrolled variations in spin rate are less than ±1%.

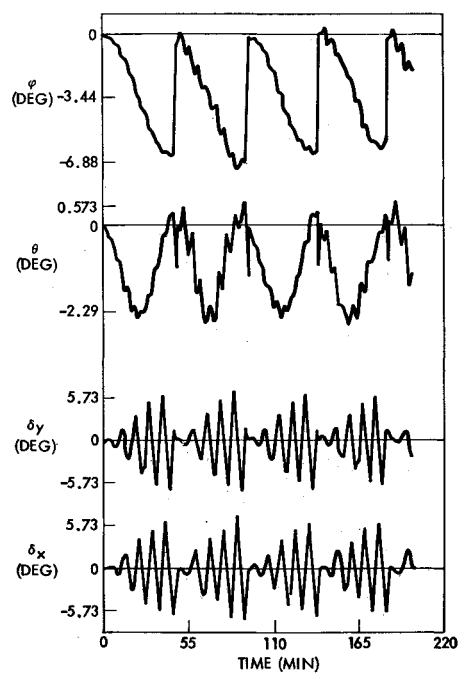

Fig. 5 Attitude errors of the spacecraft scan axis.

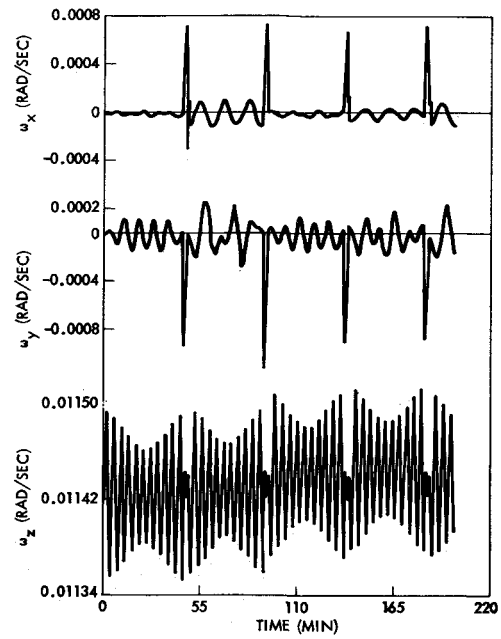

Fig. 6 Spacecraft body rates.

During the uncontrolled portion of the orbit, the secular gravity gradient torque component precesses the spacecraft z axis (and momentum vector) to a new orientation in inertial space. In each control interval (Fig. 7), the control system realigns the z axis to the nomial sun vector ($\bar{z}_i$). Each control interval is initiated during the portion of the scan cycle when the sun pointing error exists wholly about the x axis (i.e., $\delta_y = 0$ within ±0.5°). The limited slew rate about the x axis slowly rotates the spacecraft z axis back to its nominal position, during which period the y axis gyro detects the secular momentum accumulated in the previous half orbit. This momentum is simultaneously removed via the pitch thrusters. Inclusion of position control about the pitch axis ensures a terminal pitch position error within the control deadzone. Note that only 5 thruster pulses are required in pitch and 6 in roll to remove an initial attitude control error of almost 7°.

Figure 8 illustrates the spacecraft motion where the sun pointing error is computed relative to the body-fixed coordinate frame (x_b, y_b, z_b). The locus shown represents the apparent motion of the sun as viewed by an observer on the spacecraft. Near the end of each raster of 5 scans, the attitude errors are corrected and the next raster is initiated. Four complete rasters are shown in Fig. 8. Dispersion from raster

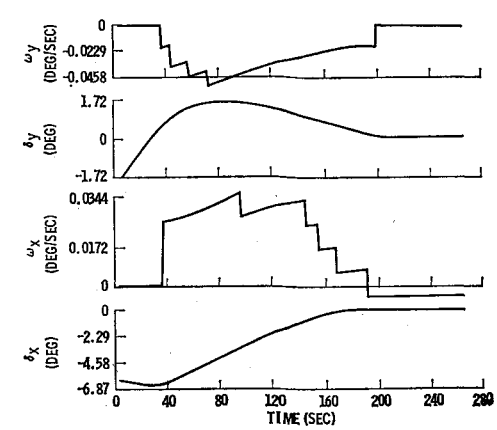

Fig. 7 Control system performance during control interval.

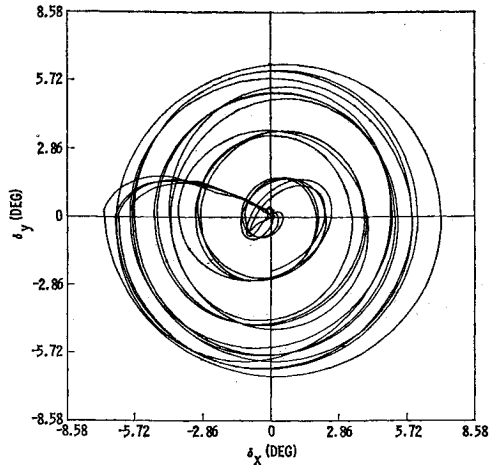

Fig. 8 Locus of the sun motion as viewed from the spacecraft.

to raster is a direct function of the control deadzones and limit cycle rates and can be decreased accordingly with the limiting factors being sun sensor noise and torquer pulse width.

Conclusions

Periodic attitude control of secular attitude errors in a slowly spinning spacecraft can be achieved via sun sensors, rate gyros and pulse-modulated mass expulsion thrusters. Periodic secular error control is attractive as control propellant is not wasted in correcting cyclic excursions of the spin-axis. Spin-axis errors during the uncontrolled periods are determined by the vehicle momentum and the magnitude of the external distrubance torques. This error can be controlled by proper selection of the spin speed and the control interval frequency.

Attitude errors at the end of each control interval are determined by the sun sensors (or the rate gyros in the offset scan mode) and control accuracies of less than 1° are readily achievable. Control parameters can be selected to yield a control efficiency in terms of propellant usage of better than 75%. The control period required is less than half the spacecraft spin period and the number of thruster firings is minimal. Phasing of the control interval to the secular error buildup in body coordinates minimizes the dynamic coupling between the x and y axes and enhances the control efficiency.

Appendix

Evaluation of the Gravity Gradient Torque

Before the gravity gradient torque can be computed, a number of coordinate frames are required to specify the parameters of the circular orbit. First, define an orthogonal inertial reference frame (x_I, y_I, z_I) as shown in Fig. 1 where $\bar{y}_I$ is normal to the equatorial plane and points northward, $\bar{z}_I$ is along the intersection of the equatorial and ecliptic planes, and $\bar{x}_I$ lies in the equatorial plane and completes the righ-handed triad. At autumnal equinox, the positive $\bar{z}_I$ axis points at the sun. Also shown in Fig. 1 is the quasi-inertial reference frame (x_i, y_i, z_i). The angle θ_s is the apparent angular displacement of the sun from its position at autumnal equinox measured in the ecliptic plane. The angle between the equatorial and ecliptic planes is 23°27′ and is denoted by γ in the subsequent analysis.

Also define an orthogonal orbital reference frame (x_r, y_r, z_r) where x_r points in the direction of the positive spacecraft velocity vector, y_r is normal to the orbit plane, z_r points down along local vertical and the origin is at the spacecraft mass center. The orbital velocity vector of the circular orbit is $\bar{\omega}_0$ (Fig. 1). Define the orientation of the orbit by the vector $\bar{z}_\beta$ along the line of nodes and the inclination of the orbit by a positive rotation (ξ) about the vector $\bar{z}_\beta$. The nodal regression angle (β) defines the position of the line of nodes in the equatorial plane relative to the z_I axis or autumnal equinox. Finally the spacecraft orbital position relative to the line of nodes is defined by an angular displacement (α) in the orbit plane as shown in Fig. 1.

The gravity gradient torque on the spacecraft (T_g) is

$$\bar{T}_g = (3g_0/S_M3)\,\bar{S}_M x(\bar{\bar{I}}\cdot\bar{S}_M) \tag{A1}$$

where g_0 is the acceleration due to gravity at the spacecraft center of mass, $\bar{S}_M$ is the displacement vector from the Earth's mass center to the spacecraft mass center and $\bar{\bar{I}}$ is the inertia dyadic of the body. Assuming negligible inertia cross-products, the inertia dyadic is

$$\bar{\bar{I}} = I_{xx}\bar{x}_b\bar{x}_b + I_{yy}\bar{y}_b\bar{y}_b + I_{zz}\bar{z}_b\bar{z}_b \tag{A2}$$

The displacement vector $\bar{S}_M$ is specified in the orbital reference frame by

$$\bar{S}_M = -S_M\bar{z}_r \tag{A3}$$

where the orientation of the orbital reference frame is defined relative to the quasi-inertial frame by

$$\begin{Bmatrix}\bar{x}_r\\ \bar{y}_r\\ \bar{z}_r\end{Bmatrix} = \begin{bmatrix}y_{11} & y_{12} & y_{13}\\ y_{21} & y_{22} & y_{23}\\ y_{31} & y_{32} & y_{33}\end{bmatrix}\begin{Bmatrix}\bar{x}_i\\ \bar{y}_i\\ \bar{z}_i\end{Bmatrix} \tag{A4}$$

The displacement vector can be expressed in body coordinates as

$$\bar{S}_M = -S_M(A\,\bar{x}_b + B\,\bar{y}_b + C\,\bar{z}_b) \tag{A5}$$

where

$$\begin{aligned} A &= y_{31}b_{11} + y_{32}b_{12} + y_{33}b_{13}\\ B &= y_{31}b_{21} + y_{32}b_{22} + y_{33}b_{23}\\ C &= y_{31}b_{31} + y_{32}b_{32} + y_{33}b_{33}\end{aligned} \tag{A6}$$

and the required elements of the Y matrix are

$$\begin{aligned} y_{31} &= S\gamma(S\alpha C\xi C\beta + C\alpha S\beta) + C\gamma S\alpha S\xi\\ y_{32} &= -C\theta_s C\gamma(S\alpha C\xi C\beta + C\alpha S\beta)\\ &\quad + C\theta_s S\gamma S\alpha S\xi - S\theta_s(S\alpha C\xi S\beta - C\alpha C\beta)\\ y_{33} &= -S\theta_s C\gamma(S\alpha C\xi C\beta + C\alpha S\beta)\\ &\quad + S\theta_s S\gamma S\alpha S\xi + C\theta_s(S\alpha C\xi S\beta - C\alpha C\beta)\end{aligned} \tag{A7}$$

Equation (A1) can now be evaluated using Eqs. (A2) and (A5) to yield the gravity gradient torque as

$$\begin{aligned}\bar{T}_g = (3g_0/S_M)[&(I_{zz} - I_{yy})BC\bar{x}_b + (I_{xx} - I_{zz})AC\bar{y}_b +\\ &(I_{yy} - I_{xx})AB\bar{z}_b)]\end{aligned} \tag{A8}$$

Consider the case where the pitch and roll errors (θ and ϕ) are zero and ψ (the spin displacement angle) is arbitrary. From Eqs. (A2) and (A8), the gravity gradient torque can be evaluated as

$$\bar{T}_g = T_{gx}\bar{x}_b + T_{gy}\bar{y}_b + T_{gz}\bar{z}_b \tag{A9}$$

where

$$\begin{aligned} T_{gx} &= K(I_{zz} - I_{yy})y_{33}(y_{32}\cos\psi - y_{31}\sin\psi)\\ T_{gy} &= K(I_{xx} - I_{zz})y_{33}(y_{31}\cos\psi + y_{32}\sin\psi)\\ T_{gz} &= K(I_{yy} - I_{xx})[y_{31}y_{32}\cos 2\psi + \tfrac{1}{2}(y_{32}^2 - y_{31}^2)\sin 2\psi]\end{aligned} \tag{A10}$$

and

$$K = 3g_0/S_M$$

The gravity gradient torque can also be expressed in terms of the quasi-inertial coordinate frame as

$$\bar{T}_g = T_{ix}\bar{x}_i + T_{iy}\bar{y}_i + T_{iz}\bar{z}_i \tag{A11}$$

where

$$T_{ix} = K[(I_{zz} - I_{yy})BCb_{11} + (I_{xx} - I_{zz})ABb_{21} + (I_{yy} - I_{xx})ABb_{31}]$$
$$T_{iy} = K[(I_{zz} - I_{yy})BCb_{12} + (I_{xx} - I_{zz})ACb_{22} + (I_{yy} - I_{xx})ABb_{32}] \quad \text{(A12)}$$
$$T_{iz} = K[(I_{zz} - I_{yy})BCb_{13} + (I_{xx} - I_{zz})ACb_{23} + (I_{yy} - I_{xx})ABb_{33}]$$

If the pitch and roll errors are again assumed zero, the gravity gradient torque components simplify to:

$$T_{ix} = Ky_{33}\left[y_{32}I_{zz} - \frac{y_{32}}{2}(I_{xx} + I_{yy}] + \frac{y_{32}}{2}(I_{xx} - I_{yy}]\cos 2\psi + \frac{y_{31}}{2}(I_{yy} - I_{xx})\sin 2\psi\right]$$
$$T_{iy} = Ky_{33}\left[\frac{y_{31}}{2}(I_{xx} + I_{yy}) - y_{31}I_{zz} + \frac{y_{32}}{2}(I_{xx} - I_{yy})\sin 2\psi + \frac{y_{31}}{2}(I_{xx} - I_{yy})\cos 2\psi\right] \quad \text{(A13)}$$
$$T_{iz} = T_{gz}$$

Averaging the torque components over a spin period yields the following average gravity gradient torque

$$\bar{T}_{ag} = T_{ax}\bar{x}_i + T_{ay}\bar{y}_i + T_{az}\bar{z}_i \quad \text{(A14)}$$

where

$$T_{ax} = KIy_{33}y_{32}$$
$$T_{ay} = KIy_{33}y_{31} \quad \text{(A15)}$$
$$T_{az} = 0$$

and

$$I = I_{zz} - (I_{xx} + I_{yy})/2 \quad \text{(A16)}$$

Secular Gravity Gradient Torque

The secular torque experienced by the vehicle is the orbital average of the gravity gradient torque. Specifically the torque components are defined as

$$T_{sx} = \frac{1}{2\pi}\int_{\alpha=0}^{2\pi} T_{ax}d\alpha = \frac{KI}{2\pi}\int_{\alpha=0}^{2\pi} y_{33}y_{32}d\alpha$$
$$T_{sy} = \frac{1}{2\pi}\int_{\alpha=0}^{2\pi} T_{ay}d\alpha = \frac{-KI}{2\pi}\int_{\alpha=0}^{2\pi} y_{33}y_{31}d\alpha \quad \text{(A17)}$$

and the secular torque magnitude (T_s) is

$$T_s = [T_{sx}^2 + T_{sy}^2]^{1/2} \quad \text{(A18)}$$

It can be shown that the secular torque has a maximum value when the angle between the sun line and orbit plane is 45° where the angle is measured in a plane normal to the orbit plane. This requirement is met whenever the spacecraft orbital parameters satisfy the following constraint equation

$$\cos\theta_s[\sin\xi \sin\beta] - \sin\theta_s[\cos\gamma \sin\xi \cos\beta + \sin\gamma \cos\xi] = \pm\cos\pi/4 \quad \text{(A19)}$$

where the plus sign is employed whenever the sun line is located above the orbit plane and the minus sign when the sun line is below the orbit plane. For a given orbital inclination and for all possible values of sun position and nodal regression angle, many instances occur when the secular torque magnitude is as its maximum value. A computer search yielded 160 specific maxima for a 28.5° orbit inclination and a ±0.1% tolerance in evaluation of the constraint equation. The quantization level on both the sun and regression angles was 1°.

The secular torque has a zero value when the sun line is within the orbit plane as the spacecraft motion is then perfectly symmetrical relative to the earth. It can be shown that the required constraint equation on the orbital parameters is

$$\tan\theta_s = \frac{\sin\beta}{\cos\gamma \cos\beta + \sin\gamma \cos\xi} \quad \text{(A20)}$$

Fig. 9 illustrates the variation in the normalized secular torque T_s/KI for nodal regression angles of 0°, 45°, 90°, 135°,

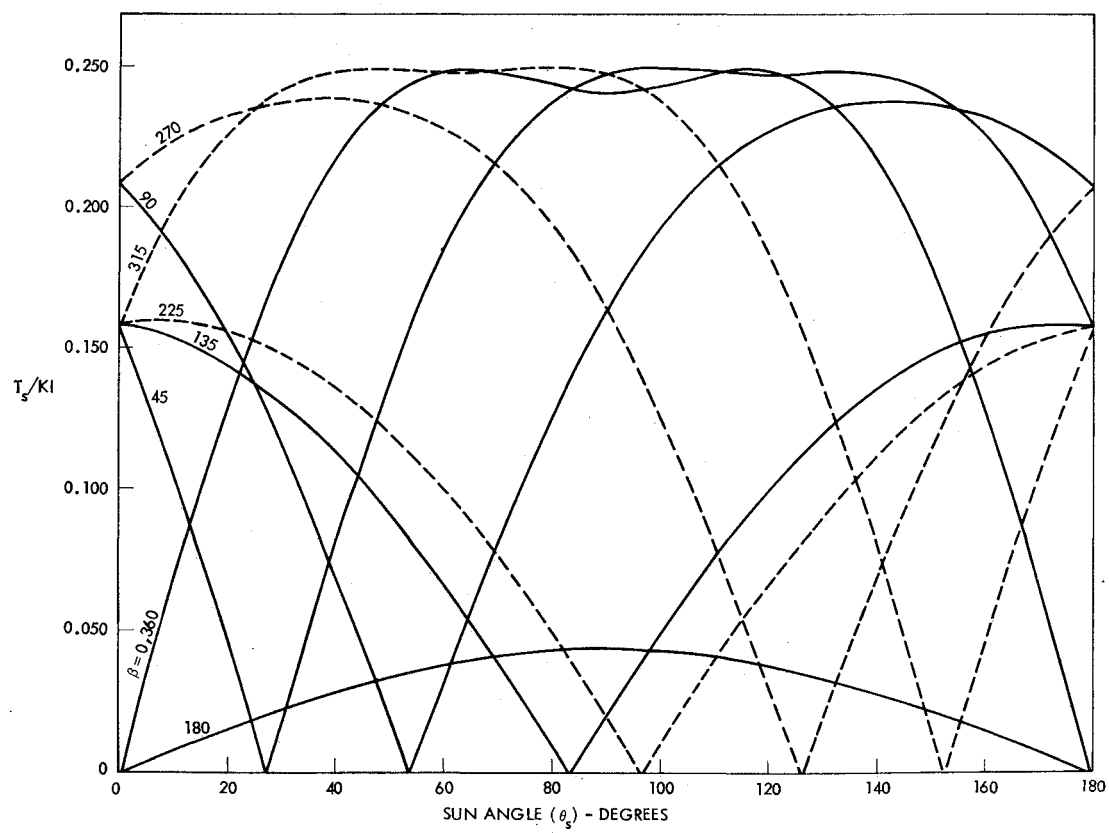

Fig. 9 Secular gravity gradient torque (normalized).

180°, 225°, 270°, 315°, and 360°. As the secular torque characteristics repeat every 180°, only the torque values for $0 < \theta_s < 180°$ are shown. For a spacecraft orbit of 200 naut miles ($K = 3.90 \times 10^{-6}$ rad/sec^2) and the example spacecraft ($I = 2.66 \times 10^4$ slug-ft^2), the peak secular torque is 2.60×10^{-2} ft-lb.

References

[1] Wheeler, P. C., "Two-Pulse Attitude Control of an Asymmetric Spinning Satellite," *Progress in Astronautics and Aeronautics. Guidance and Control—II*, edited by R. C. Langford and C. J. Mundo, Vol. 13, Academic Press, New York, 1964, pp. 261–287.

[2] Patapoff, H., "Bank Angle Control System for a Spinning Satellite," *Progress in Astronautics and Aeronautics. Guidance and Control—II*, edited by R. C. Langford and C. J. Mundo, Vol. 13, Academic Press, New York, 1964, pp. 289–312.

[3] Carrier, G. F. and Miles, J. W., "On the Annular Damper for a Freely Precessing Gyroscope," *Journal of Applied Mechanics*, June 1960, pp. 237–240.

[4] Bhuta, P. G. and Koval, L. R., "A Viscous Ring Damper for a Freely Precessing Satellite," *International Journal of Mechanical Sciences*, Vol. 8, 1966, pp. 383–395.

NOVEMBER 1973 J. SPACECRAFT VOL. 10, NO. 11

Maneuver Design and Implementation for the Mariner 9 Mission

R. T. MITCHELL* AND W. J. O'NEIL†
Jet Propulsion Laboratory, Pasadena, Calif.

The maneuver strategy and operational techniques employed in controlling the Mariner 9 flight path from Earth launch, through interplanetary space, Mars orbit insertion, and the subsequent orbital trim maneuvers are presented. It is shown how the maneuver strategy was tailored to meet the mission requirements with maximum reliability in the presence of launch vehicle injection, orbit determination, and spacecraft maneuver execution errors as great as 3σ.

I. Introduction

THE first section of this paper presents a description of the mission design as it relates to the development of specific navigation requirements. Orbit determination and maneuver execution accuracy statistics are used in conjunction with the total velocity increment constraint to determine specific maneuver requirements.

The second section describes the design of each maneuver, the selection of target parameters, the minimization of the effects of execution errors, and the actual inflight results. The impact of each maneuver on subsequent maneuvers is discussed.

II. Maneuver Strategy

Mission Design

One of the primary objectives of the Mariner 9 mission to Mars was to perform a detailed mapping of the Martian surface with contiguous television pictures having a resolution of 1 km or better over the latitude band from $-60°$ to $+40°$. Due to the 0.6 hr difference between the rotational periods of Earth and Mars, it is possible to synchronize the period of revolution of a Mars orbiter with an Earth tracking station and also have a migration of the orbiter's surface track which is very favorable for mapping—about 9° of Mars longitude per day.

The Mariner 9 mission design capitalized on this fortuitous circumstance by selecting an orbital period of about 12 hr so that every other periapsis passage would occur near the middle of the Mars view period from the tracking station at Goldstone, Calif. The view periods were just long enough to play back a full spacecraft tape recorder load of 32 pictures to the 64-m Goldstone antenna, record another 32 picture swath near periapsis, and then immediately play back the new load before the end of the tracking period. The spacecraft tape recorder was then empty and ready to record another 32 picture load at the next periapsis, which would not occur during a Goldstone view period.

The spacecraft propellant load required to achieve the desired 12 hr Mars orbit stressed the Atlas/Centaur launch vehicle's payload capability for the mission to the point that only 60 m/sec spacecraft velocity capability was available for midcourse and orbital trim maneuvers. Therefore, minimization of the total velocity requirement was a prime consideration in determining the maneuver strategy.

Navigation Requirements

For reasons of over all reliability it was a goal to minimize the number of maneuvers. Furthermore, to avoid disrupting the mapping activity during the prime orbital mission, which by definition was the first 90 days in orbit, any necessary orbital trim maneuvers were to be completed during the 8 days immediately following orbit insertion. In order to achieve satisfactory synchronization with the Goldstone view period it was required that the time of periapsis passage following the trim maneuver(s) occur within the 1 hr "window" immediately following Goldstone zenith. Because the duration of the Goldstone view period would increase gradually throughout

Presented as Paper 72-913 at the AIAA/AAS Astrodynamics Conference, Palo Alto, Calif., September 11–12, 1972; submitted October 26, 1972; revision received June 22, 1973. This paper presents the results of work carried out at the Jet Propulsion Laboratory, California Institute of Technology under Contract NAS 7-100, sponsored by NASA.

Index categories: Unmanned Lunar and Interplanetary Systems; Spacecraft Navigation, Guidance, and Flight-Path Control Systems.

* Supervisor, Viking Maneuver Group.

† Chief, Flight Path Analysis Viking Project.